



Title	Molecule-like structure with covalent neutrons of F isotopes toward the neutron drip line
Author(s)	Kimura, M. ; Furutachi, N.
Citation	Physical Review C, 83(4), 044304 https://doi.org/10.1103/PhysRevC.83.044304
Issue Date	2011-04
Doc URL	https://hdl.handle.net/2115/45302
Rights	©2011 American Physical Society
Type	journal article
File Information	PRC83-4_044304.pdf



Molecule-like structure with covalent neutrons of F isotopes toward the neutron drip line

M. Kimura

Creative Research Initiative (CRIS), Hokkaido University, Sapporo 001-0021, Japan

N. Furutachi

Meme Media Laboratory, Hokkaido University, Sapporo 060-8628, Japan

(Received 18 January 2011; published 5 April 2011)

The α -cluster structure of F isotopes has been studied based on antisymmetrized molecular dynamics. By using the constraint on the principal quantum number, various neutron configurations are investigated. It is found that a proton excitation into an sd shell does not necessarily induce α clustering in ^{21}F and ^{23}F . However, once one or two neutrons are excited into the pf shell together with a proton excitation, the core nuclei have α clustering. The calculation is extended toward the neutron drip line. The neutron-rich F isotopes also have α clustering in the excited states and their excitation energy greatly decreases toward the neutron drip line. The relation between the reduction of their excitation energies and the breaking of the neutron magic number $N = 20$ is suggested.

DOI: [10.1103/PhysRevC.83.044304](https://doi.org/10.1103/PhysRevC.83.044304)

PACS number(s): 21.10.-k, 21.60.Gx

I. INTRODUCTION

Study of neutron-rich unstable nuclei has revealed their exotic structure and binding mechanism. For example, the properties of ^{31}Na [1,2] have shown the breakdown of the magic number $N = 20$ in neutron-rich nuclei. Due to strong deformation of the system, the intruder configuration in which neutrons are excited across the $N = 20$ shell gap dominates the ground band [3] and is called the “island of inversion.” Nowadays, systematic breaking of the magic number $N = 20$ in the neighboring nuclei of ^{31}Na has been theoretically studied [4–10] and many observations have been made [11–14].

In addition to the shell structure the cluster structure also plays an important role in neutron-rich nuclei. The best example is the molecule-like structure of neutron-rich Be isotopes. Antisymmetrized molecular dynamics (AMD) [15–17] has shown that all of Be isotopes have the 2α core surrounded by valence neutrons. The motion of valence neutrons is well understood by the concept of molecular orbits [18–20]. By assuming the presence of a 2α -cluster core and covalent neutrons occupying so-called π and σ molecular orbits, their properties are also reasonably described [21,22]. The pronounced 2α clustering of ^{11}Be and ^{12}Be that leads to the breaking of the magic number $N = 8$ is also discussed. These results suggest a novel binding mechanism and exotic clustering peculiar to $N \neq Z$ nuclei.

Recently, the experimental and theoretical exploration of molecule-like structure with covalent neutrons has been rapidly developing. Molecule-like states with covalent neutrons in O, Ne, and Mg isotopes are suggested by von Oertzen [23]. Along with this suggested scenario, the experimental survey for those cluster states has been performed. It has been found that ^{18}O [24] and ^{21}Ne [25] have candidates of the molecule-like structure in their excited states. On the theoretical side, cluster-model calculations [26–28] and AMD calculations [29,30] have been reproduced and predicted the

various kinds of cluster states with covalent neutrons. Thus the cluster state with covalent neutrons in O and Ne isotopes is one of the fascinating topics in $N \neq Z$ nuclei.

In this study, we discuss the molecule-like structure of F isotopes based on the AMD calculation. The α -cluster states in ^{19}F have been investigated theoretically and experimentally in detail in the 1970s. Cluster-model calculations [31,32] have shown that once a proton is excited into the sd shell from the p shell, four nucleons in the sd shell have a strong α correlation and the α -cluster bands emerge. The lowest $\alpha + ^{15}\text{N}$ band, $K^\pi = 1/2_1^-$, is built on the famous low-lying $1/2_1^-$ state at 110 keV and its parity partner, the $K^\pi = 1/2_1^+$ band, is built on the $1/2_2^+$ state at 5.3 MeV. In contrast to ^{19}F , α clustering of heavier F isotopes is rather obscure. To our knowledge, there are no cluster-model studies for ^{21}F and α -cluster states have not been identified experimentally yet. There is almost no theoretical or experimental information about heavier F isotopes. Our aim in this study is to investigate the α clustering and molecule-like structure in heavier F isotopes and extend it toward the neutron drip line.

It will be shown that in the excited states of ^{21}F and ^{23}F there are several molecule-like states with different configuration of valence neutrons. It is found that a proton excitation into the sd shell does not necessarily induce α clustering in ^{21}F and ^{23}F . However, once one or two neutrons are excited into the pf shell together with a proton excitation, the core nuclei have α clustering. The calculation is extended toward the neutron drip line. The neutron-rich F isotopes also have α clustering in the excited states and their excitation energy greatly decreases toward the neutron drip line. The relation between the reduction of their excitation energies and the breaking of the neutron magic number $N = 20$ is suggested.

This paper is organized as follows. In the next section, we briefly explain the theoretical framework of the AMD + generator coordinate method (GCM). In Sec. III, we discuss the α -cluster states of ^{19}F and molecule-like states of

^{21}F and ^{23}F . The α -cluster states in neutron-rich nuclei from ^{25}F to ^{29}F are also discussed. The final section summarizes this work.

II. THEORETICAL FRAMEWORK

We perform a variational calculation after parity projection under constraints on deformation and the principal quantum number of a harmonic oscillator. After the variation, we project an eigenstate of total angular momentum. Finally, we superpose them and diagonalize the Hamiltonian. This calculational procedure is the same as that used in the previous work [29].

A. Wave function and effective interaction

The intrinsic wave function of the system with mass A is given by a Slater determinant of single-particle wave packets,

$$\Phi_{\text{int}} = \mathcal{A}\{\varphi_1, \varphi_2, \dots, \varphi_A\}, \quad \varphi_i(\mathbf{r}) = \varphi_i(\mathbf{r})\chi_i\xi_i, \quad (1)$$

where φ_i is the i th single-particle wave packet consisting of the spatial φ_i , spin χ_i , and isospin ξ_i parts. The local Gaussian located at \mathbf{Z}_i is employed as [33]

$$\begin{aligned} \varphi_i(\mathbf{r}) &= \exp\left[-\sum_{\sigma=x,y,z} \nu_\sigma \left(r_\sigma - \frac{Z_{i\sigma}}{\sqrt{\nu_\sigma}}\right)^2\right], \\ \chi_i &= \alpha_i\chi_\uparrow + \beta_i\chi_\downarrow, \quad |\alpha_i|^2 + |\beta_i|^2 = 1, \\ \xi_i &= \text{proton or neutron.} \end{aligned} \quad (2)$$

Here \mathbf{Z}_i , α_i , β_i , and ν_σ are the variational parameters. The parity-projected wave function, $\Phi^\pi = \hat{P}^\pi \Phi_{\text{int}}$, is the variational wave function.

The Gogny DIS force [34] is employed as an effective nuclear force \hat{V}_n and the Coulomb force \hat{V}_C is approximated by a sum of seven Gaussians.

B. Variation under constraints

In the present work, two kinds of constraints on the variational wave function are imposed simultaneously. The first is the constraint on the matter quadrupole deformation β as given in Ref. [35].

Another is the constraint on the number of the deformed harmonic oscillator quanta, which is called the N constraint in the following. The number operator is defined for protons and neutrons as

$$\hat{N}^{(p,n)} = \sum_{i \in p,n} \sum_{\sigma=x,y,z} \left(\frac{p_{\sigma i}^2}{4\hbar\nu_\sigma} + \nu_\sigma r_{\sigma i}^2 \right) - \frac{3}{2}. \quad (3)$$

We impose some different constraints on the expectation values $N^\xi = \langle \Phi^\pm | \hat{N}^\xi | \Phi^\pm \rangle / \langle \Phi^\pm | \Phi^\pm \rangle$. For example, by adding the potential

$$\begin{aligned} V_N &= v_N (N^\xi - N_0)^2 \theta(N^\xi - N_0), \\ \theta(x) &= \begin{cases} 0, & x < 0, \\ 1, & x \geq 0, \end{cases} \quad v_N > 0, \end{aligned} \quad (4)$$

to the energy of the system, N^ξ is restricted to less than N_0 . Details of the applied N constraints are explained in the next section.

Variational parameters are optimized by the frictional cooling method so that the energy of the system plus constraint potentials is minimized and we obtain the optimized wave function $\Phi_{\text{int}}^\pm(\{C\})$ under a certain combination of β - and N -constraint parameters $\{C\}$.

C. Analysis of the single-particle orbit

To investigate the motion of the valence neutrons, we calculate the single-particle orbit in the optimized wave function $\Phi_{\text{int}}^\pm(\{C\})$. We transform the single-particle wave packet φ_i to the orthonormalized basis, $\tilde{\varphi}_\alpha = \frac{1}{\sqrt{\lambda_\alpha}} \sum_{i=1}^A c_{i\alpha} \varphi_i$. Here, λ_α and $c_{i\alpha}$ are the eigenvalues and eigenvectors of the overlap matrix $B_{ij} = \langle \varphi_i | \varphi_j \rangle$. By using this basis, the Hartree-Fock single-particle Hamiltonian,

$$\begin{aligned} h_{\alpha\beta} &= \langle \tilde{\varphi}_\alpha | \hat{h} | \tilde{\varphi}_\beta \rangle + \sum_{\gamma=1}^A \langle \tilde{\varphi}_\alpha \tilde{\varphi}_\gamma | \hat{v}_n + \hat{v}_c | \tilde{\varphi}_\beta \tilde{\varphi}_\gamma - \tilde{\varphi}_\gamma \tilde{\varphi}_\beta \rangle \\ &+ \frac{1}{2} \sum_{\gamma,\delta=1}^A \langle \tilde{\varphi}_\gamma \tilde{\varphi}_\delta | \tilde{\varphi}_\alpha \tilde{\varphi}_\beta \frac{\partial \hat{v}_n}{\partial \rho} | \tilde{\varphi}_\gamma \tilde{\varphi}_\delta - \tilde{\varphi}_\delta \tilde{\varphi}_\gamma \rangle, \end{aligned} \quad (5)$$

is calculated. The eigenvalues ϵ_s and eigenvectors $f_{\alpha s}$ of $h_{\alpha\beta}$ give the single-particle energies and the single-particle orbits, $\tilde{\varphi}_s = \sum_{\alpha=1}^A f_{\alpha s} \tilde{\varphi}_\alpha$.

D. Angular momentum projection and GCM

After the variational calculation, we project out an eigenstate of the total angular momentum J ,

$$\Phi_{MK}^{J\pm}(\{C\}) = \hat{P}_{MK}^J \Phi^\pm(\{C\}). \quad (6)$$

Here \hat{P}_{MK}^J is the total angular momentum projector. The integrals over three Euler angles are evaluated by the numerical integration.

Finally, the wave functions $\Phi_{MK}^{J\pm}(\{C\})$ which have the same parity and angular momentum but have different K and constraint parameters $\{C\}$ are superposed (GCM). Then the wave function of the system is written as

$$\Phi_n^{J\pm} = c_n \Phi_{MK}^{J\pm}(\{C\}) + c'_n \Phi_{MK'}^{J\pm}(\{C'\}) + \dots, \quad (7)$$

where the quantum numbers except for the total angular momentum and the parity are represented by n . The coefficients c_n, c'_n, \dots are determined by the Hill-Wheeler equation.

III. RESULTS AND DISCUSSION

The α clustering in ^{19}F has been well established and is known, while those of neutron-rich isotopes are rather obscure. We first demonstrate how the α clustering of ^{19}F is described in the present framework. Then, we investigate the level structure of ^{21}F and ^{23}F and discuss their α -cluster states. Finally, α -cluster states toward the neutron drip line are studied and their relation to the breaking of magic number $N = 20$ is suggested.

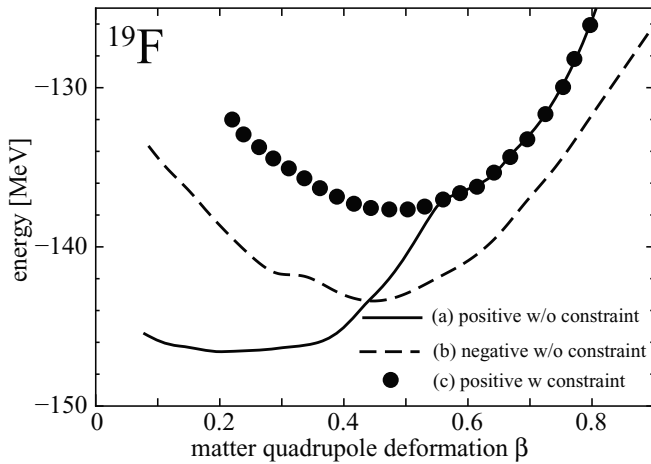


FIG. 1. Energy curves of ^{19}F calculated with and without the N constraint. The solid and dashed lines show the energy curves of the positive- and negative-parity states, respectively, obtained without the N constraint. The circle shows that of the positive-parity state obtained with the N constraint.

A. ^{19}F

Many cluster-model studies [31,32] have shown that the $K^\pi = 1/2^-$ and $1/2_2^+$ bands of ^{19}F have prominent $\alpha + ^{15}\text{N}$ cluster structure and constitute a parity doublet. When a proton is excited into the sd shell across the $Z = 8$ magic number, four nucleons in the sd shell have a strong α correlation and an $\alpha + ^{15}\text{N}$ cluster structure develops. An important fact for the present study is that the α -cluster states of ^{19}F have a proton hole in the p shell.

Keeping this in mind, we look at the result obtained by AMD. Solid and dashed lines in Fig. 1 show the energy curves obtained without the N constraint. The positive-parity state has a minimum at $\beta = 0.2$ and the corresponding intrinsic density distribution is shown in Fig. 2(a). This state generates the ground band after the GCM calculation. Its density distribution

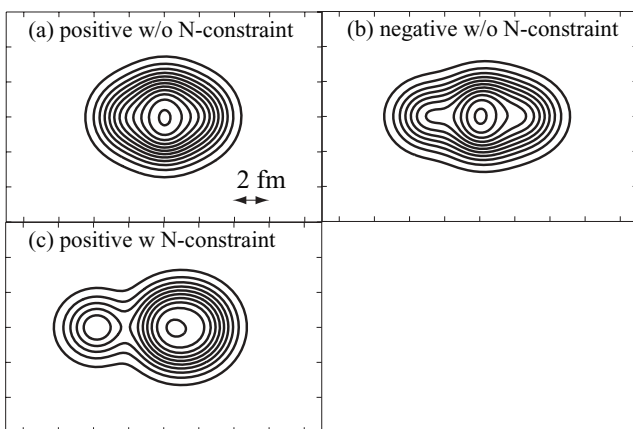


FIG. 2. Intrinsic density distributions of ^{19}F at energy minima on the energy curves. Figures (a) and (b), respectively, show positive- and negative-parity minima obtained without the N constraint. Figure (c) shows the positive-parity minimum obtained with the N constraint.

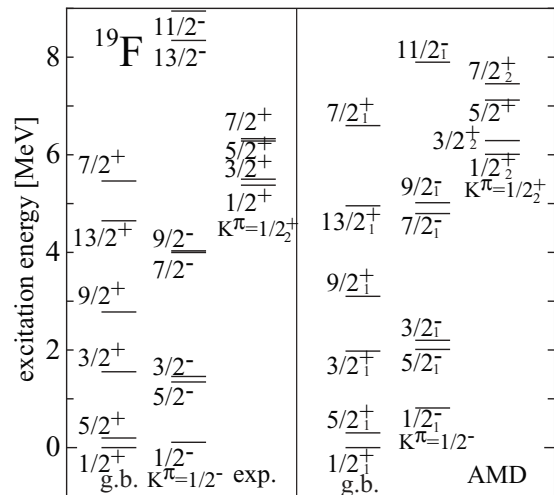


FIG. 3. Calculated (right) and corresponding observed (left) partial level schemes of ^{19}F . Experimental data are taken from Refs. [36–38].

shows the absence of α clustering in the ground band. The projection to the negative-parity state brings about the structure change, because a proton excitation into the sd shell occurs. The negative-parity state has a strongly deformed minimum at $\beta = 0.45$. Its density [Fig. 2(b)] exhibits the $\alpha + ^{15}\text{N}$ clustering and this state constitutes the $K^\pi = 1/2^-$ band. The parity partner of the $K^\pi = 1/2^-$ band is obtained by using the N constraint. Filled circles in Fig. 1 show the energy curve of the positive-parity state with the N constraint. Here N^p is restricted to more than 9 (with the lowest Pauli allowed value being 8) and it forces a proton excitation into the sd shell. The energy curve obtained with the N constraint shows that a shoulder of the energy curve without the N constraint belongs to a different energy curve with different particle-hole configuration. This configuration has a local minimum at $\beta = 0.45$. Its density distribution [Fig. 2(c)] shows the prominent $\alpha + ^{15}\text{N}$ clustering of this state. Thus

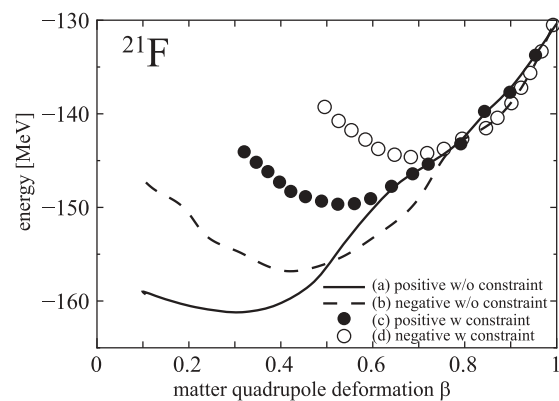


FIG. 4. Energy curves of ^{21}F calculated with and without the N constraint. Solid and dashed lines show the curves of the positive- and negative-parity states, respectively, obtained without the N constraint. Filled and open circles show that of the positive- and negative-parity states, respectively, with the N constraint.

a proton excitation is essential to induce the α clustering of ^{19}F and it is controlled well by applying the N constraint.

We performed a GCM calculation by superposing all wave functions on the energy curves. Figure 3 shows the calculated and corresponding observed partial level scheme of ^{19}F [36–38]. We obtained the ground band and two excited rotational bands ($K^\pi = 1/2^-$ and $1/2_2^+$). There also exists the $K^\pi = 1/2_2^-$ band at 11 MeV (called the ‘‘higher-nodal band’’) but is out of the energy range in Fig. 3. Two excited rotational bands dominantly consist of the wave functions that have $\alpha + ^{15}\text{N}$ cluster structure, while the ground band is dominated by a $(sd)^3$ configuration. All of them show reasonable agreement with the experimental data in their energies, moments of inertia, and decoupling parameters, though the excitation energies of the α -cluster bands are overestimated by about 0.8 MeV.

B. ^{21}F

To our knowledge, the α -cluster structure of ^{21}F has not been studied and looks obscure. Experimental information is also rather poor, and there are only several states with definite spin and parity assignment. Encouraged by the successful description of ^{19}F , we investigate the α -cluster structure of ^{21}F by using the N constraint.

Figure 4 shows the energy curves obtained with and without the N constraint. The positive-parity curve without the N constraint (solid line) has a minimum at $\beta = 0.3$ and a shoulder around $\beta = 0.65$. The density distribution at the minimum is

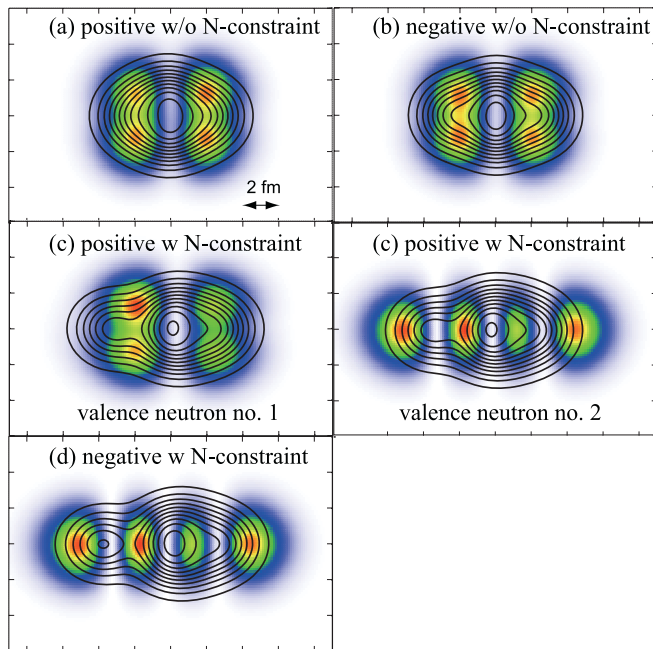


FIG. 5. (Color online) Intrinsic density distributions of ^{21}F at energy minima on the energy curves. Solid line shows the density of the core (^{19}F) and the color plot shows that of the valence neutrons. Figures (a) and (b), respectively, show positive- and negative-parity minima obtained without the N constraint. Figures (c) and (d), respectively, show the positive- and negative-parity minima obtained with the N constraint.

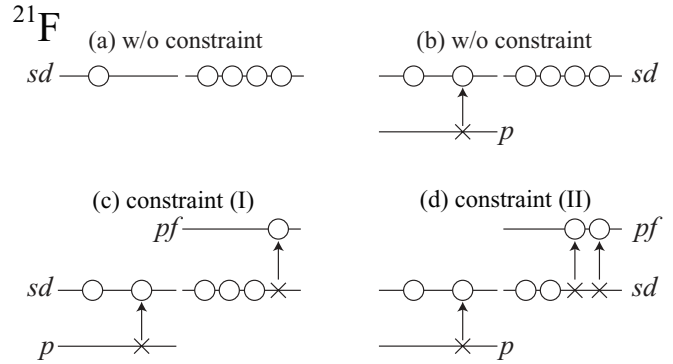


FIG. 6. Schematic illustration of the single-particle configurations of ^{21}F obtained by the variational calculations with and without the N constraint.

shown in Fig. 5(a). Here the density of the valence neutrons is defined as the most weakly bound two-neutron density, and the density of the core is defined as the density of all remaining nucleons. We can see that there is no α clustering of the core and the valence neutrons occupy the $d_{5/2}$ orbit. The analysis of the single-particle orbit shows that this state has the configuration illustrated in Fig. 6(a) in a simple shell-model picture. In the literature of the Nilsson model, this orbit is denoted as $[N, n_z, l_z, j_z] = [2, 2, 1, 3/2]$. The negative-parity curve (dashed line) has a minimum at $\beta = 0.42$ and a shoulder around $\beta = 0.8$. The density distribution at the minimum [Fig. 5(b)] and the analysis of the single-particle orbit show that the valence neutrons occupy the same orbit with the positive-parity state and a proton is excited into the sd shell from the p shell [Fig. 6(b)]. It must be noted that a proton excitation into the sd shell does not necessarily induce α clustering different from that seen in ^{19}F . This is due to the two-neutron occupation of the $[2, 2, 1, 3/2]$ orbit. Since the binding energy of this orbit decreases as prolate deformation becomes larger, it prevents the α clustering that brings about strong prolate deformation.

The situation changes dramatically when one or two valence neutrons are excited into the pf shell together with a proton excitation from the p to the sd shell. We have applied two different N constraints. Constraint I is applied to the positive-parity state and forces a proton excitation into the sd shell ($N^p > 9$) and a neutron excitation into the pf shell ($N^n > 15$; the lowest Pauli allowed value being 14). Constraint II is applied to the negative-parity state and forces a proton excitation ($N^p > 9$) and two-neutron excitation into the pf shell ($N^n > 16$). These constraints, respectively, generate the configurations illustrated in Figs. 6(c) and 6(d) in a simple shell-model picture. The positive-parity energy curve with the N constraint (filled circles) has a minimum at $\beta = 0.41$. Its density distribution [Fig. 5(c)] shows the $\alpha + ^{15}\text{N}$ clustering of the core. In this configuration, one of two valence neutrons occupies the $[2, 2, 1, 3/2]$ orbit [Fig. 5(c), left] as in the ground state and another neutron occupies the pf shell $[[3, 3, 0, 1/2]$, Fig. 5(c), right]. It must be noted that once a neutron is excited into the pf shell together with a proton excitation into the sd shell, the core has α clustering. Since the binding energy of the last neutron orbit $[3, 3, 0, 1/2]$ becomes larger, it prefers

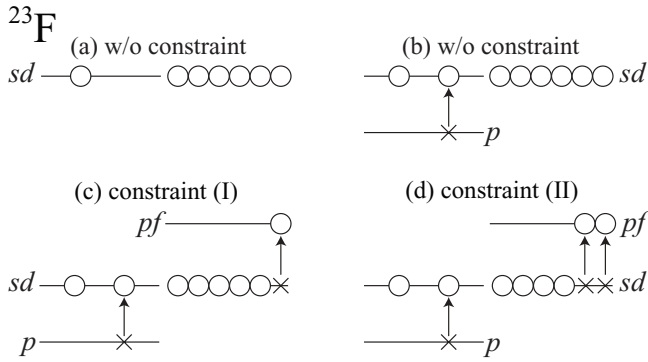


FIG. 9. Same as Fig. 6 but for ^{23}F .

the shoulders on the energy curves obtained without the N constraint have different structure from the minima, and the configurations (c) and (d) have their own minima at $\beta = 0.5$. Their density distributions [Figs. 10(c) and 10(d)] show α clustering. Again we see that once one or two neutrons are excited into the $[3, 3, 0, 1/2]$ orbit, the α cluster develops. In the case of the positive-parity state, one neutron occupies the $[3, 3, 0, 1/2]$ orbit [Fig. 10(c), right] and moderate α clustering occurs. In the case of the negative-parity state, two neutrons occupy the $[3, 3, 0, 1/2]$ orbit and the α clustering is enhanced in the positive-parity state. Though the number of the valence neutrons is increased, the occupation of the $[3, 3, 0, 1/2]$ orbit brings about a result similar to that of ^{21}F . However, we note that the deformation of these α -cluster states is smaller than those of ^{21}F , being due to the occupation of the $[2, 1, 1, 3/2]$ orbit. If we consider ^{23}F as a $^{19}\text{F} + 4n$ system, two of four valence neutrons always occupy the $[2, 1, 1, 3/2]$ orbit and another two neutrons change their occupation depending on the N constraint. As we have seen in the case of ^{21}F , the $[2, 1, 1, 3/2]$ orbit tends to reduce the deformation of the

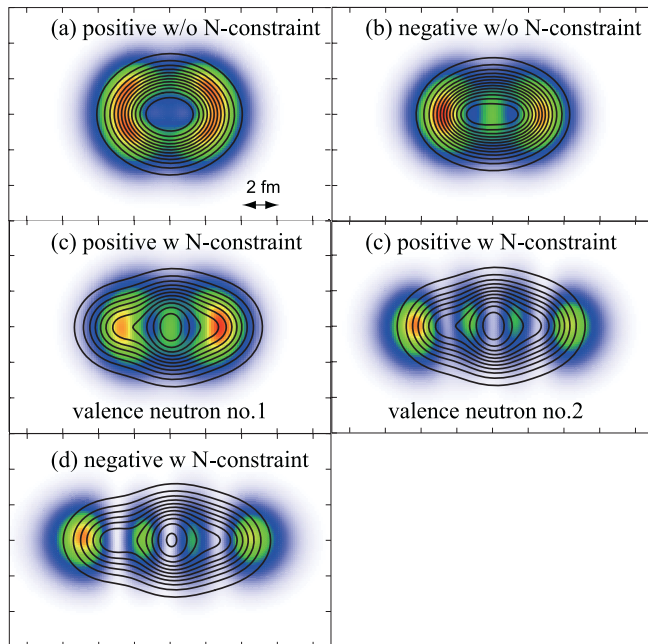


FIG. 10. (Color online) Same as Fig. 5 but for ^{23}F .

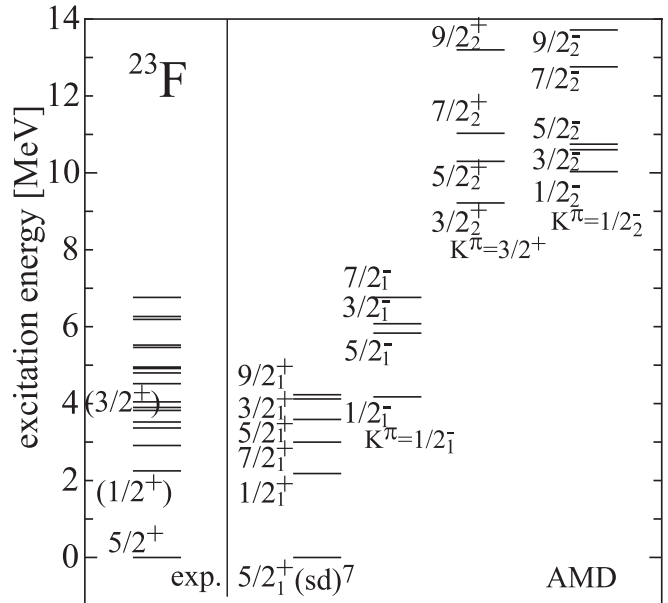


FIG. 11. Same as Fig. 7 but for ^{23}F . Experimental data are taken from Ref. [43].

system, while the $[3, 3, 0, 1/2]$ orbit and α clustering of the core increase it. The detailed balance between them determines the deformation of the α -cluster states.

Figure 11 shows the level scheme of ^{23}F . Experimental information [43] is completely deficient. About 20 states are observed but only the ground state has a definite spin-parity assignment. We have obtained three rotational bands together with the states with $(sd)^7$ configuration. The ground state is the $5/2_1^+$ state with $(sd)^7$ configuration and agrees with the observation. The observed states at 2.3 and 4.0 MeV are tentatively assigned as $1/2_1^+$ and $3/2_1^+$ [44], which agree well with the present result ($1/2_1^+$ at 2.2 MeV and $3/2_1^+$ at 4.2 MeV). Several states are observed in this energy region and many of them may be classified as an $(sd)^7$ configuration. The negative-parity states with a configuration illustrated in Fig. 9(b) appear between 4 and 7 MeV. Their experimental counterpart is unclear, though there are about 10 states observed in this energy region. We note that the excitation energy of the lowest negative-parity state increases as a function of neutron number. In our calculation they are, respectively, 0.9, 2.6, and 4.1 MeV in ^{19}F , ^{21}F , and ^{23}F and observed at 0.1 and 1.1 MeV in ^{19}F and ^{21}F . The increase of the excitation energy is understood as follows. All these states have a proton excitation into the sd shell and neutrons have the lowest-energy configurations. In the case of the ^{19}F , since a proton excitation immediately leads to the strong α correlation, it does not cost much energy. By increasing the neutron number, α clustering is suppressed due to the valence neutron orbit and the excitation energy becomes larger. Since the α clustering of the core strongly depends on the valence neutron configuration, the excitation energy of the proton-hole state will be sensitive to the motion of valence neutrons and the α clustering of the core. This point is discussed in the next section.

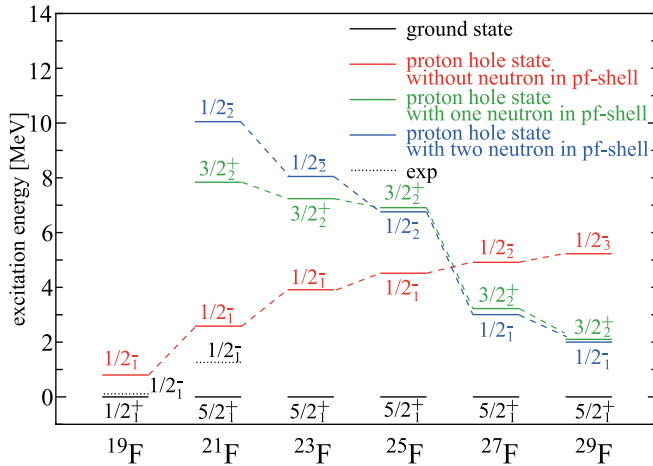


FIG. 12. (Color online) Excitation energies of the bandhead states with proton-hole configurations without a neutron in the pf shell (red), with a neutron in the pf shell (green), and with two neutrons in the pf shell (blue) in F isotopes.

D. α -cluster states near the drip line and relation to the breaking of magic number $N = 20$

To illustrate the α clustering toward the neutron drip line, we have performed the same calculation for $^{25,27,29}\text{F}$. Namely, by using the N constraint, we have calculated the proton-hole states without neutrons in the pf shell and with one or two neutrons in the pf shell. ^{31}F was unbound in the present model. This contradicts observation [45] and is not discussed here.

For each proton-hole configuration, we have obtained a corresponding excited rotational band as in the cases of ^{21}F and ^{23}F . Detailed discussion on individual isotopes will be made in our future work and we focus here on their bandhead states. Figure 12 shows the excitation energies of the bandhead states. In all calculated isotopes, the proton-hole configuration without neutrons in the pf shell generates the $K^\pi = 1/2^-$ band (red lines) and the proton-hole configurations with one or two neutrons in the pf shell, respectively, generate the $K^\pi = 3/2^+$ and $1/2^-$ bands (green and blue lines).

Similar to ^{21}F and ^{23}F , the proton-hole states without neutrons in the pf shell do not have α -cluster structure. Since the number of valence neutrons in the sd shell is increased, deformation of the system is suppressed and α clustering is seriously diminished. Their excitation energies are gradually increased as a function of neutron number. The structure of these states is basically understood as the $0p_{1/2}$ proton-hole states coupled to the ground state of Ne isotopes except for ^{29}F . Since ^{30}Ne is located in the island of inversion, two neutrons occupy the pf shell in the ground state, and the $N = 20$ closed-shell configuration appears as the excited states. Therefore, a proton-hole state of ^{29}F without a neutron in the pf shell corresponds to a proton-hole state coupled to the excited state of ^{30}Ne .

Once one or two neutrons are excited into the pf shell together with a proton excitation into the sd shell, the system is strongly deformed and the α -cluster structure develops. Different from the $\alpha + ^{15}\text{N}$ cluster states of ^{19}F , these cluster states have an α -cluster structure surrounded by valence

neutrons and manifest a strong coupling nature rather than a weakly bound two-body cluster structure. They show a dramatic reduction of their excitation energies toward the drip line. The reasons for this reduction are as follows. (1) As the number of neutrons increases, the excitation energy needed to promote neutrons into the pf shell decreases. This is simply due to the increase of neutron Fermi energy. (2) In the case of $^{27,29}\text{F}$ ($N = 18$ and 20), they are located around or inside of the island of inversion. In this mass region, the ground state is strongly deformed and neutrons occupy the pf shell due to the reduction of the $N = 20$ shell gap. We recall that the neutron intruder orbit in the island of inversion is nothing but the $[3, 3, 0, 1/2]$ orbit [10] discussed up to now. Therefore, the energy required for neutron excitation is greatly reduced from that of lighter isotopes. Especially, a proton-hole configuration of ^{29}F with two neutrons in the pf shell is understood as a $0p_{1/2}$ proton hole coupled to the ground state of ^{30}Ne , since two neutrons occupy the pf shell in the ground state of ^{30}Ne . The neutron excitation into the pf shell brings about strong deformation and α clustering to the system; then the strong deformation further reduces the neutron single-particle energy of the $[3, 3, 0, 1/2]$ orbit. Thus the neutron excitation and α clustering of the core work in a cooperative way and reduce the energies of the $2\hbar\omega$ and $3\hbar\omega$ excited states $[\pi(1\hbar\omega) \otimes \nu(1 \text{ or } 2\hbar\omega)]$. It is noted that in Ref. [46] a couple of low-lying states of ^{25}F and ^{27}F are observed. They reported that these states are not reproduced by an sd - pf shell model that does not include proton excitation and pointed out the possibility of the proton and neutron excitation in these states. Further detailed study for individual isotopes will be our next work and more experimental information is required to investigate the present scenario.

IV. SUMMARY

In summary, we have investigated the α -cluster structure of F isotopes based on antisymmetrized molecular dynamics. By using the N constraint, we have controlled proton and neutron configurations. The well-known α -cluster states of ^{19}F with a proton hole in the p shell are successfully described. In the case of ^{21}F and ^{23}F , a proton excitation does not immediately lead to α clustering of the core. When one or two valence neutrons occupy the pf shell ($[3, 3, 0, 1/2]$ orbit) together with a proton excitation, the core has α clustering and strong deformation. These α -cluster states appear as the excited rotational bands around 7 to 10 MeV. The calculation is extended to $^{25,27,29}\text{F}$. We only have discussed the excitation energies of the $1/2^-$ state with a proton hole, the $3/2^+$ state with a proton hole and a neutron in the pf shell, and the $1/2^-$ state with a proton hole with two neutrons in the pf shell. While the excitation energy of the state without neutron excitation increases toward the drip line, those with neutrons in the pf shell decrease drastically. This reduction may be related to the breakdown of the neutron magic number $N = 20$ near the drip line. Further theoretical investigation will be made in our next work and more experimental information is required to understand α clustering near the drip line.

- [1] C. Thibault *et al.*, *Phys. Rev. C* **12**, 644 (1975).
- [2] G. Huber *et al.*, *Phys. Rev. C* **18**, 2342 (1978).
- [3] E. K. Warburton, J. A. Becker, and B. A. Brown, *Phys. Rev. C* **41**, 1147 (1990).
- [4] A. Poves and J. Retamosa, *Phys. Lett. B* **184**, 311 (1987).
- [5] N. Fukunishi, T. Otsuka, and T. Sebe, *Phys. Lett. B* **296**, 279 (1992).
- [6] R. R. Rodriguez-Guzman, J. L. Egido, and L. M. Robledo, *Phys. Rev. C* **62**, 054319 (2000).
- [7] M. Kimura and H. Horiuchi, *Prog. Theor. Phys. (Kyoto)* **107**, 33 (2002).
- [8] Y. Utsuno, T. Otsuka, T. Glasmacher, T. Mizusaki, and M. Honma, *Phys. Rev. C* **70**, 044307 (2004).
- [9] M. Kimura and H. Horiuchi, *Prog. Theor. Phys. (Kyoto)* **111**, 841 (2004).
- [10] M. Kimura, *Phys. Rev. C* **75**, 041302 (2007).
- [11] T. Motobayashi *et al.*, *Phys. Lett. B* **346**, 9 (1995).
- [12] K. Yoneda *et al.*, *Phys. Lett. B* **499**, 233 (2001).
- [13] S. Nummela *et al.*, *Phys. Rev. C* **64**, 054313 (2001).
- [14] G. Neyens *et al.*, *Phys. Rev. Lett.* **94**, 022501 (2005).
- [15] Y. Kanada-En'yo, H. Horiuchi, and A. Doté, *Phys. Rev. C* **60**, 064304 (1999).
- [16] Y. Kanada-En'yo and H. Horiuchi, *Phys. Rev. C* **66**, 024305 (2002).
- [17] Y. Kanada-En'yo and H. Horiuchi, *Phys. Rev. C* **68**, 014319 (2003).
- [18] Y. Abe, J. Hiura, and H. Tanaka, *Prog. Theor. Phys. (Kyoto)* **49**, 800 (1973).
- [19] M. Seya, M. Kohno, and S. Nagata, *Prog. Theor. Phys. (Kyoto)* **65**, 204 (1981).
- [20] W. von Oertzen, *Z. Phys. A* **354**, 37 (1996).
- [21] N. Itagaki and S. Okabe, *Phys. Rev. C* **61**, 044306 (2000).
- [22] N. Itagaki, S. Okabe, and K. Ikeda, *Phys. Rev. C* **62**, 034301 (2000).
- [23] W. von Oertzen, *Eur. Phys. J. A* **11**, 403 (2001).
- [24] W. von Oertzen *et al.*, *Eur. Phys. J. A* **43**, 17 (2010).
- [25] C. Wheldon *et al.*, *Eur. Phys. J. A* **26**, 321 (2005).
- [26] P. Descouvemont and D. Baye, *Phys. Rev. C* **31**, 2274 (1985).
- [27] P. Descouvemont, *Phys. Rev. C* **38**, 2397 (1988).
- [28] M. Dufour and P. Descouvemont, *Nucl. Phys. A* **726**, 53 (2003).
- [29] M. Kimura, *Phys. Rev. C* **75**, 034312 (2007).
- [30] N. Furutachi, M. Kimura, A. Doté, Y. Kanada-En'yo, and S. Oryu, *Prog. Theor. Phys.* **119**, 403 (2008).
- [31] T. Sakuda and F. Nemoto, *Prog. Theor. Phys. (Kyoto)* **62**, 1274 (1979); **62**, 1606 (1979).
- [32] P. Descouvemont and D. Baye, *Nucl. Phys. A* **463**, 629 (1987).
- [33] M. Kimura, *Phys. Rev. C* **69**, 044319 (2004).
- [34] J. Dechargé and D. Gogny, *Phys. Rev. C* **21**, 1568 (1980).
- [35] A. Doté, H. Horiuchi, and Y. Kanada-En'yo, *Phys. Rev. C* **56**, 1844 (1997).
- [36] D. R. Tilley *et al.*, *Nucl. Phys. A* **595**, 1 (1995).
- [37] S. Mordechai and H. T. Fortune, *Phys. Rev. C* **29**, 1765 (1984).
- [38] D. M. Pringle and W. J. Vermehr, *Nucl. Phys. A* **499**, 117 (1989).
- [39] R. B. Firestone, *Nucl. Data Sheets* **103**, 269 (2004).
- [40] G. Mairle *et al.*, *Z. Phys. A* **301**, 157 (1981).
- [41] M. G. Silbert and N. Jarmie, *Phys. Rev.* **123**, 221 (1961).
- [42] P. von Neumann-Cosel, R. Jahn, U. Fister, T. K. Trelle, and B. A. Brown, *Phys. Rev. C* **56**, 547 (1997).
- [43] R. B. Firestone, *Nucl. Data Sheets* **108**, 1 (2007).
- [44] S. Michimasa *et al.*, *Phys. Lett. B* **638**, 146 (2006).
- [45] H. Sakurai *et al.*, *Phys. Lett. B* **448**, 180 (1999).
- [46] Z. Elekes *et al.*, *Phys. Lett. B* **599**, 17 (2004).